Journal of Power Sources 195 (2010) 5735–5748

Contents lists available at ScienceDirect

Journal of Power Sources

journal homepage: www.elsevier.com/locate/jpowsour

Electric powertrain modeling of a fuel cell hybrid electric vehicle and development of a power distribution algorithm based on driving mode recognition

Junghwan Ryu, Yeongseop Park, Myoungho Sunwoo*

Hanyang University, 17 Haengdang-dong, Seongdong-gu, Seoul 133-791, Republic of Korea

ARTICLE INFO

Article history:
Received 18 December 2009
Received in revised form 25 February 2010
Accepted 9 March 2010
Available online 2 April 2010

Keywords:
Fuel cell hybrid electric vehicle
Power distribution algorithm
Fuzzy controller
Adaptive membership function
Driving pattern recognition

ABSTRACT

This paper proposes a novel fuzzy controller based on an adaptive membership function for optimum power management of a fuel cell hybrid electric vehicle (FCHEV). In the first phase, an electric powertrain model of the FCHEV is derived and a fuzzy controller is proposed. Then, the fuzzy controller is optimized using a genetic algorithm. The optimization process is accomplished through simulation for a given driving cycle. Since, however, the optimized result may vary according to the applied driving cycle for optimization, it is impossible for one optimized result to cover various driving cycles. In the second phase, an adaptive membership function based on a stochastic approach is proposed to guarantee optimum performance from the presented fuzzy controller, even though the driving cycle changes. This controller is referred to as the 'Stochastic fuzzy controller' (SFC) in this study. The SFC employs a stochastic approach where membership functions can be transformed statistically using a probability evaluated from driving pattern recognition. Then, driving cycle analysis is performed through off-line simulation and hardware in a loop simulation (HILS) test for four driving cycles. Finally, the SFC shows the best performance in terms of minimum fuel consumption and state-of-charge (SoC) maintenance.

1. Introduction

Today, local air pollution and climate change caused by conventional vehicles threaten the continuous existence of human beings on Planet Earth. To ameliorate these problems, many countries have implemented various environmental friendly policies. These efforts have motivated the introduction of hybrid vehicles to resolve energy and environment problems. Generally, a hybrid vehicle is powered by an internal combustion engine (ICE) and a battery [1]. Nevertheless, there still exists a possibility of increasing air pollution and global warming because an ICE is used. Among the alternative power sources for ICEs, the most promising device is a fuel cell. Fuel cells can generate electricity without the emission of harmful exhaust gases such as NOx, HC, with pure water being the only reaction product. In addition, fuel cells have a higher efficiency than ICEs. Thus, many automotive companies have developed a fuel cell vehicle.

These fuel cell vehicles have a hybrid configuration with a battery and/or a supercapacitor. The additional power source not only prevents the oxygen starvation problem in the fuel cell (if oxygen is starved, the cell voltage falls to very low levels or may even become negative and irreversible damage may eventuate [2]) but also offers the potential of higher performance and better fuel economy. In addition, hybridization of a fuel cell stack with a battery or a supercapacitor decreases the size and the cost of the fuel cell stack system [3]. Such a vehicle is called a fuel cell hybrid electric vehicle (FCHEV).

In hybrid vehicles, power distribution between two power sources is an important factor for minimum fuel consumption and the maintenance of battery state-of-charge (SoC). For power distribution, several heuristic approaches have been proposed [4,5] and use a rule-based algorithm that can be described by using a state flow. The fuel cell is operated in a highly efficient range, and an additional power source, either a battery or a supercapacitor, accommodates the load leveling range [6,7]. A fuzzy controller also has been developed by many research groups [8–14]. Since, however, it is derived from intuition or heuristic knowledge, this strategy cannot guarantee optimum power distribution. Accordingly, many research groups have published other optimum power control strategies using dynamic programming (DP) [1], stochastic dynamic programming (SDP) [15–17], equivalent consumption minimization (ECMS) [18,19], and an optimized fuzzy controller with a genetic algorithm (GA) [20–23]. All of these optimum power control strategies have been developed using a mathematical model of the hybrid vehicle.

* Corresponding author. Tel.: +82 2 2220 0453; fax: +82 2 2297 5495.
E-mail addresses: yesican@hanyang.ac.kr (J. Ryu), autopark@hanyang.ac.kr (Y. Park), msunwoo@hanyang.ac.kr (M. Sunwoo).

0378-7753/$ – see front matter © 2010 Elsevier B.V. All rights reserved.
doi:10.1016/j.jpowsour.2010.03.081

Nomenclature

C	capacity [F]
d	duty
i	current [A]
GLEPK	GLEPK [L 100 km^{-1}]
L	inductance [H]
LHV	low heating value [J g^{-1}]
MPGGE	MPGGE [mpg]
N	number of data
$nGene$	number of genes
nP	number of individuals
SoC	state-of-charge
o	optimization design variables
p	probability
P	power [W]
Q	charge [C]
r	electrical resistance [Ω]
t	time [s]
u	input vector
v	voltage [V]
W	mass flow rate [kg s^{-1}]

Greek letters

ρ	density [g L^{-1}]
η	efficiency
γ	scaling coefficient of probability revision function
λ_a	scaling coefficient of probability revision function

Subscripts

batt	battery
bus	bus line
B	battery
C	capacitor
DCDC	d.c.–d.c. converter
f	final time
Gas	gasoline
HWFET	HWFET driving cycle
int	internal component
load	load
L	inductor or linearization
max	maximum value
mov	moving value (moving average or standard deviation)
MF	membership function
oc	open circuit
ref	reference value
req	required value
SFC	stochastic fuzzy controller
SoCref	SoC reference value
st	fuel cell stack
target	fuel cell stack
u	input
UDDS	UDDS driving cycle
0	initial value

Superscripts

avg	average value
desired	desired value
modified	required value
ref	reference value
STD	standard deviation

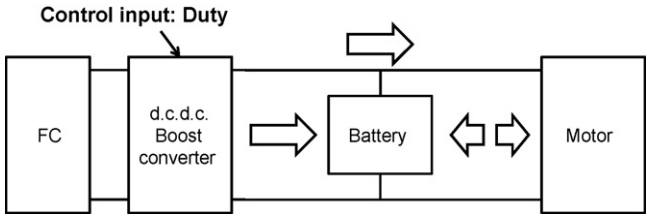

Fig. 1. Parallel-type FCHEV configuration.

Power control strategies for FCHEV have been developed using static or non-causal electric powertrain models [5,16,17,19,23]. These models cannot describe the dynamic characteristics of the electric powertrain, such as bus voltage and fuel cell current behaviour. In following papers [16,17], the bus voltage and the battery current were calculated using a static equation for a given battery power; this is non-causal. Uzunoglu and Alam [23] used an ideal d.c.–d.c. converter model which neglects the effects of parasitic elements [24]. Haitao et al. [25] a dynamic model of the electric powertrain but it was obtained using simplified first-order transfer functions. Therefore, in this study an electric powertrain model of the FCHEV is formulated from dynamic differential equations of an equivalent circuit model that represents the electric powertrain.

As mentioned above, it is considerably important to prevent oxygen starvation through management of fuel cell current. Most power control strategies for FCHEVs have disregarded the oxygen starvation problem [5,14,23], or applied an indirect current management method; the derivative value of the fuel cell power was limited instead of the fuel cell current [15–17,19,25]. Therefore, in this research, a power control strategy, which can modulate the utilization of the fuel cell current directly, has been developed and implemented using a fuzzy control algorithm. Then, using a genetic algorithm process, membership functions (MFs) of the fuzzy controller are optimized for given driving cycles, in order to achieve minimum fuel consumption and maintenance of the battery SoC.

For the power management of the FCHEV, DP, SDP, pseudo-SDP and fuzzy optimized using GA can be obtained through the optimization process for a given driving cycle. Since, however, the optimized result vary according to the applied driving cycle for optimization, these approaches cannot guarantee accurate results for other driving cycles. In order to solve this problem, a power control strategy, which can be used in various driving cycles, is proposed. This has been realized using a fuzzy controller based on adaptive membership functions. The controller is referred to as the 'Stochastic fuzzy controller' (SFC) in this study.

This paper presents the dynamic electric powertrain of a parallel-type FCHEV and demonstrates the operating mechanism of the SFC. In the first part, an electric powertrain model is derived from an equivalent circuit model and a power distribution algorithm using a fuzzy controller is proposed. In addition, the optimization process of the fuzzy controller using GA, is reported. In the second part of the paper, the operating mechanism of the SFC is detailed and a probability evaluation method is proposed to achieve the accurate adjustment of MFs. Finally, the performance of the SFC is validated through simulation and hardware in a loop simulation (HILS) [26,27].

2. FCHEV configuration

The FCHEV has several configurations according to the topology of the power sources, types and sizes. A parallel hybrid type was adopted, as shown in Fig. 1. In this structure, the fuel cell power, which is supplied to a battery and/or a traction motor, can be controlled using a d.c.–d.c. converter. Specifically, the current from the fuel cell stack can be governed by controlling the d.c.–d.c. converter.

Unlike a configuration which has no a d.c.–d.c. converter, this type of FCHEV prevents the abrupt current draw from the fuel cell, and thus solves the oxygen starvation problem.

3. Electric powertrain model of parallel hybrid type FCHEV

In this study, the electric powertrain model of the FCHEV consists of three components: a dynamic fuel cell stack system model, a d.c.–d.c. converter and a battery model.

3.1. Fuel cell stack system model

The model of the fuel cell stack system derived by Pukrushpan et al. [28] was used in this study. The model is composed of auxiliary components and the fuel cell stack and was obtained for the 75 kW stack in the FORD P2000 fuel cell prototype vehicle. The auxiliary components support efficient and effective operation of the fuel cell. The subsystems of the auxiliary components are a compressor, a supply manifold, an air cooler and humidifier, and a return manifold. It is assumed that the air cooler and humidifier maintain the temperature and humidity of the air entering the stack at constant values of 80 °C and 100% respectively. Additionally, the stack temperature is assumed to be held constant at 80 °C by a well-designed cooling subsystem. This is because the change in stack temperature is relatively slow.

The fuel cell stack model integrates a stack voltage model, a cathode flow model and an anode flow model. The type of fuel cell is a polymer electrolyte fuel cell (PEFC). Accordingly, the water content in the PEFC dominates the performance of the fuel cell [29]. It is assumed that the membrane is always hydrated in vapour equilibrium state, so that the water content in the membrane is maintained at 14 [30]. A fuel cell stack has many cells to increase the voltage that are connected in series. It is assumed that the performance of each cell is uniform, and that the stack voltage is calculated by the product of the number of cells and the voltage of a single cell.

3.2. d.c.–d.c. converter model

In order to raise the fuel cell stack voltage, a boost-type d.c.–d.c. converter [31] can be utilized. The dynamic behaviour of the boost converter is determined according to the commutation mode of the transistor [31] and its mathematical model can be obtained by applying Kirchhoff's voltage and current laws (KVL and KCL).

3.3. Battery model

The battery type was a 25 kW Li-ion unit from ADVISOR [32]. An internal resistance model described the chemical behaviours of the battery using an electrical equivalent circuit as if it were a perfect open-circuit voltage (OCV) source in a series with an internal resistance.

3.4. State–space model of FCHEV electric powertrain

By integrating the three electric component models the electric powertrain was constructed, as shown in Fig. 2. A traction motor acts as a load and was represented as a current source. The load current (i_{load}) was varied with the required power to drive the FCHEV.

In accord with modeling of the d.c.–d.c. converter, the equivalent circuit model can also be analyzed by the commutation mode of the transistor. When the transistor is ON, the equations related to the inductor current (i_{st}) and capacitor voltage (v_C) are obtained by the

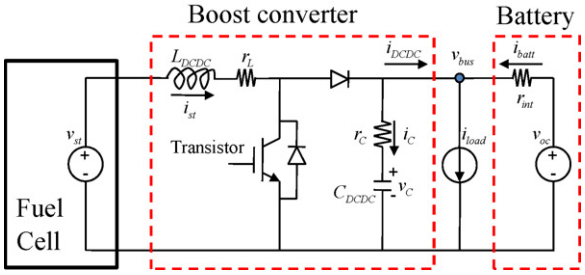

Fig. 2. The equivalent circuit model of the electric powertrain.

KVL and KCL, as expressed by:

$$v_{st} = L_{DCDC}\frac{di_{st}}{dt} + r_L i_{st}, \tag{1}$$

$$\begin{aligned} &v_{oc} = r_{int} i_{batt} + v_{bus},\ v_{bus} = r_C i_C + v_C, \\ &v_{oc} = r_{int}(i_{load} + i_C) + r_C i_C + v_C, \\ &C_{DCDC}\frac{dv_C}{dt} = -\frac{1}{r_{int}+r_C}v_C - \frac{r_{int}}{r_{int}+r_C}i_{load} + \frac{1}{r_{int}+r_C}v_{oc}. \end{aligned} \tag{2}$$

When the transistor is OFF, the following equations are derived by the KVL and KCL:

$$v_{st} = L_{DCDC}\frac{di_{st}}{dt} + r_L i_{st} + v_{bus} = L_{DCDC}\frac{di_{st}}{dt} + r_L i_{st} + r_C C_{DCDC}\frac{dv_C}{dt} + v_C, \tag{3}$$

$$\begin{aligned} &i_{st} + i_{batt} = i_C + i_{load},\ i_{batt} = \frac{v_{oc} - v_{bus}}{r_{int}}, \\ &C_{DCDC}\frac{dv_C}{dt} = \frac{r_{int}}{r_{int}+r_C}i_{st} - \frac{1}{r_{int}+r_C}v_C - \frac{r_{int}}{r_{int}+r_C}i_{load} + \frac{1}{r_{int}+r_C}v_{oc}. \end{aligned} \tag{4}$$

Finally, considering d, the commutation mode of the transistor [33], the derivatives of the inductor current and the capacitor voltage can be calculated using Eqs. (5) and (6):

$$\begin{aligned} \frac{di_{st}}{dt} = &\left\{-\frac{r_L}{L_{DCDC}} - \frac{r_{int}r_C(1-d)}{(r_{int}+r_C)L_{DCDC}}\right\} i_{st} + \left(-1 + \frac{r_C}{r_{int}+r_C}\right)\frac{v_C(1-d)}{L_{DCDC}} \\ &+ \frac{r_{int}r_C(1-d)}{(r_{int}+r_C)L_{DCDC}} i_{load} + \frac{v_{st}}{L_{DCDC}} - \frac{r_C(1-d)}{(r_{int}+r_C)L_{DCDC}} v_{oc}, \end{aligned} \tag{5}$$

$$\begin{aligned} \frac{dv_C}{dt} = &\frac{r_{int}(1-d)}{r_{int}+r_C}\frac{i_{st}}{C_{DCDC}} - \frac{1}{r_{int}+r_C}\frac{v_C}{C_{DCDC}} \\ &- \frac{r_{int}}{r_{int}+r_C}\frac{i_{load}}{C_{DCDC}} + \frac{1}{r_{int}+r_C}\frac{v_{oc}}{C_{DCDC}}. \end{aligned} \tag{6}$$

As you can see in Eqs. (5) and (6), variable d can determine the fuel cell current (i_{st}) and the capacitor voltage (v_C) Thus it is possible to control the fuel cell power to load and/or battery using variable d. Therefore, d is the control input of the FCHEV electric powertrain. A real control system of the d.c.–d.c. converter generates d which takes the value 1 or 0 and has a high frequency of more than several tens of kHz. This research concentrates on the development of an efficient power distribution controller to achieve minimum fuel consumption and maintain the battery SoC during vehicle operation. To do this, simulation work is performed for given driving cycles of the vehicle. Since, however, driving cycles have running times of more than hundreds of seconds and d should be updated with a time step of hundreds of microseconds, the simulation time becomes very long. In order to reduce the simulation time, an average value model was used in which the control input d takes a value

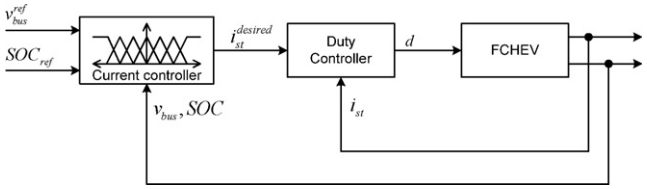

Fig. 3. The control strategy using the fuzzy controller.

of between 0 and 1 and matches the duty ratio (commutation period of the transistor) [33]. Thus, the simulation work could be performed without considering switching operation. It is reasonable to use an average value model, because research is focused on the development of a power distribution controller and not switching control of the d.c.–d.c. converter.

Next, the state–space model (Eq. (7)) of the FCHEV electric powertrain was formulated from Eqs. (5) and (6):

$$\begin{bmatrix} \dot{i}_{st} \\ \dot{v}_C \end{bmatrix} = \begin{bmatrix} -\frac{r_L}{L_{DCDC}} - \frac{r_{int}r_C(1-d)}{(r_{int}+r_C)L_{DCDC}} & \left(-1+\frac{r_C}{r_{int}+r_C}\right)\frac{(1-d)}{L_{DCDC}} \\ \frac{r_{int}(1-d)}{r_{int}+r_C} & -\frac{1}{r_{int}+r_C} \end{bmatrix} \begin{bmatrix} i_{st} \\ v_C \end{bmatrix} + \begin{bmatrix} \frac{r_{int}r_C(1-d)}{(r_{int}+r_C)L_{DCDC}} & \frac{1}{L_{DCDC}} & -\frac{r_C(1-d)}{(r_{int}+r_C)L_{DCDC}} \\ -\frac{r_{int}}{r_{int}+r_C C_{DCDC}} & 0 & \frac{1}{(r_{int}+r_C)C_{DCDC}} \end{bmatrix} \begin{bmatrix} i_{load} \\ v_{st} \\ v_{oc} \end{bmatrix}. \quad (7)$$

Moreover, the bus voltage and the battery current were obtained using these states and input variables, as given by:

$$\begin{bmatrix} v_{bus} \\ i_{batt} \end{bmatrix} = \begin{bmatrix} \frac{r_{int}r_C(1-d)}{r_{int}+r_C} & \frac{r_{int}}{r_{int}+r_C} \\ \frac{-r_C(1-d)}{r_{int}+r_C} & \frac{-1}{r_{int}+r_C} \end{bmatrix} \begin{bmatrix} i_{st} \\ v_C \end{bmatrix} + \begin{bmatrix} -\frac{r_{int}r_C}{r_{int}+r_C} & 0 & \frac{r_C}{r_{int}+r_C} \\ \frac{r_C}{r_{int}+r_C} & 0 & \frac{1}{r_{int}+r_C} \end{bmatrix} \begin{bmatrix} i_{load} \\ v_{st} \\ v_{oc} \end{bmatrix}. \quad (8)$$

In order to include the SoC as one of states in the state–space model, the relation of the SoC and the battery current was obtained as follows:

$$\mathrm{SoC}(t) = \mathrm{SoC}_0 - \frac{\eta_{batt}}{Q_{max}}\int_0^t i_{batt}dt, \qquad \frac{d\mathrm{SoC}(t)}{dt} = -\frac{\eta_{batt}}{Q_{max}} i_{batt}. \quad (9)$$

Therefore, the derivative of the SoC can be inserted into the state–space model as shown by:

$$\begin{bmatrix} \dot{i}_{st} \\ \dot{v}_C \\ \dot{\mathrm{SoC}} \end{bmatrix} = \begin{bmatrix} -\frac{r_L}{L_{DCDC}} - \frac{r_{int}r_C(1-d)}{(r_{int}+r_C)L_{DCDC}} & \left(-1+\frac{r_C}{r_{int}+r_C}\right)\frac{(1-d)}{L_{DCDC}} & 0 \\ \frac{r_{int}(1-d)}{(r_{int}+r_C)C_{DCDC}} & -\frac{1}{(r_{int}+r_C)C_{DCDC}} & 0 \\ \frac{r_C(1-d)\times\eta_{batt}}{Q_{max}(r_{int}+r_C)} & \frac{1\times\eta_{batt}}{Q_{max}(r_{int}+r_C)} & 0 \end{bmatrix} \begin{bmatrix} i_{st} \\ v_{oc} \\ \mathrm{SoC} \end{bmatrix} + \begin{bmatrix} \frac{r_{int}r_C(1-d)}{(r_{int}+r_C)L_{DCDC}} & \frac{1}{L_{DCDC}} & -\frac{r_C(1-d)}{(r_{int}+r_C)L_{DCDC}} \\ -\frac{r_{int}}{(r_{int}+r_C)C_{DCDC}} & 0 & \frac{1}{(r_{int}+r_C)C_{DCDC}} \\ \frac{-r_C\times\eta_{batt}}{Q_{max}(r_{int}+r_C)} & 0 & \frac{-1\times\eta_{batt}}{Q_{max}(r_{int}+r_C)} \end{bmatrix} \begin{bmatrix} i_{load} \\ v_{st} \\ v_{oc} \end{bmatrix}, \quad (10)$$

$$\begin{bmatrix} v_{bus} \\ i_{batt} \end{bmatrix} = \begin{bmatrix} \frac{r_{int}r_C(1-d)}{r_{int}+r_C} & \frac{r_{int}}{r_{int}+r_C} & 0 \\ \frac{-r_C(1-d)}{r_{int}+r_C} & \frac{-1}{r_{int}+r_C} & 0 \end{bmatrix} \begin{bmatrix} i_{st} \\ v_C \\ \mathrm{SoC} \end{bmatrix} + \begin{bmatrix} -\frac{r_{int}r_C}{r_{int}+r_C} & 0 & \frac{r_C}{r_{int}+r_C} \\ \frac{r_C}{r_{int}+r_C} & 0 & \frac{1}{r_{int}+r_C} \end{bmatrix} \begin{bmatrix} i_{load} \\ v_{st} \\ v_{ss} \end{bmatrix}. \quad (11)$$

4. Fuzzy controller for power distribution in FCHEV

In this study, the fuzzy controller has been proposed to achieve lower fuel consumption and SoC maintenance of the FCHEV; the control strategy is shown in Fig. 3. The fuzzy controller generates a desired fuel cell current instead of the desired fuel cell power. This control scheme has been used in two previous studies for the FCHEV power distribution control [16,17]. This is because the dynamic fuel cell stack system model [28] was employed in the research. The dynamic fuel cell stack system model requires the fuel cell current as an input instead of the power. Actually, the fuel cell power can be controlled by modulating the fuel cell current.

The above method, however, was modified to control the increment of the fuel cell current. The fuzzy controller decides the derivative value of the desired fuel cell current ($di_{st}^{desired}/dt$) to prevent an abrupt change in the desired fuel cell current. In the previous studies [13–16], the fuel cell stack was operated without quick generation of fuel cell power, because of oxygen starvation or a compressor choke. In fact, the most direct cause of the above problems is not quick power generation but abrupt increase in fuel cell current. This is due to the fact that air mass flow into the fuel cell is determined by the stoichiometry ratio and fuel cell current [28]. Accordingly, in this research, the fuzzy controller is designed to determine the derivative value of the fuel cell current. A maximum of the derivative value is limited at a high value where oxygen is not starved. Then, the desired fuel cell current is calculated by integrating the derivative value (see Fig. 4).

In previous researches on FCHEVs [14,16,17,19], the required power and the SoC were used for inputs. The required power, however, cannot provide information about variation in the required power. It is necessary to know the variation of the required power so as to generate the desired derivative value of the fuel cell current. Thus, the required power should be differentiated. Since differentiation is sensitive to sensor noise, however, it is needed to avoid differentiation. Hence, in this research, the bus voltage is used instead of differentiation of the required power. If the required power increases abruptly, there is a large fall in bus voltage. Conversely, a rapid decline in the required power causes a large increase in bus voltage. When the battery absorbs regenerative braking energy, the bus voltage also rises. This control concept offers a fundamental reason why a dynamic electric powertrain model has to be used; previously, the power control strategies were designed using static or quasi-static powertrain models, which could not describe the behaviour of the bus voltage. Thus, it is impossible to design power control strategies that can consider the bus voltage of the electric powertrain.

Finally, the fuzzy controller inputs are the bus voltage of the electric powertrain and the current SoC level of the battery. Using these two states, the fuzzy controller determines the required current from the fuel cell. It is then delivered to the duty controller for regulating the d.c.–d.c. converter, as shown in Fig. 3. The duty controller yields the duty ratio to track the desired fuel cell current.

The difference from the reference value of each control target state (the bus voltage and the SoC) can offer information pertaining to high or low current states. Thus, the inputs of the fuzzy controller are the bus voltage error and the SoC error. The errors are defined as:

$$e\mathrm{SoC} = \mathrm{SoC}_{ref} - \mathrm{SoC}, \quad eV = v_{bus}^{ref} - v_{bus}. \quad (12)$$

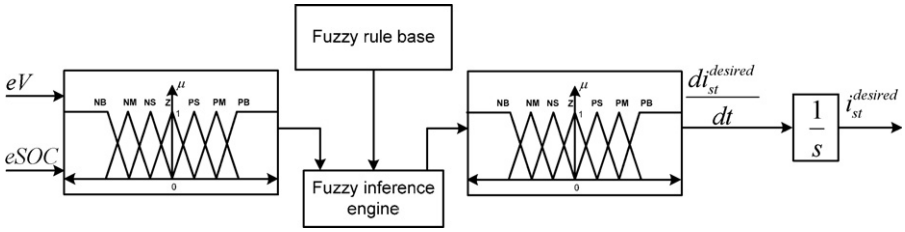

Fig. 4. The internal structure of the fuzzy controller.

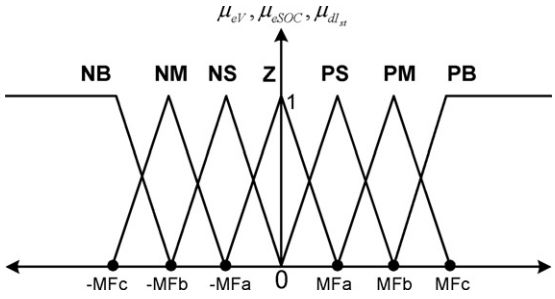

Fig. 5. The points of the MF for *eV*, *e*SoC, and di_{st}.

The internal structure of the fuzzy controller is depicted in Fig. 4.

Regarding the fuzzy controller, the rule base has to be defined to represent the human knowledge needed for controlling a target system [34]. For the power distribution of the FCHEV, this study derived the fuzzy rule base which can satisfy the required power and maintain the battery SoC using the above two inputs. For example, if the SoC level and the bus voltage are higher than their respective reference values, the fuel cell current can be decreased. On the contrary, if the SoC and the bus voltage are lower than the references, a high increase of the fuel cell current may be needed to satisfy both the bus voltage regulation and the SoC maintenance. An abrupt increase in the power supplied from the fuel cell, however, should be avoided. These strategies, which are derived from the knowledge based on the physical phenomena of the electric circuit, become the fuzzy rule base. In this study, the MFs of the fuzzifier and defuzzifier have a common structure, which is composed of the triangular membership illustrated in Fig. 5. Using the linguistic variables from each of the MFs and above strategies, the IF-THEN rules can be derived and then rearranged as shown in Table 1.

5. Optimization of fuzzy controller using a genetic algorithm

A genetic algorithm is a search technique developed to find an exact or approximate solution for optimization or a search problem. In this study, a GA was employed to find an optimized MF set for the fuzzy controller.

Table 1
Rule base.

*e*SoC							
eV	NB	NM	NS	Z	PS	PM	PB
NB	NB	NB	NB	NB	NM	NS	Z
NM	NB	NB	NB	NM	NS	Z	PS
NS	NB	NB	NM	NS	Z	PS	PM
Z	NB	NM	NS	Z	PS	PM	PB
PS	NM	NS	Z	PS	PM	PB	PB
PM	NS	Z	PS	PM	PB	PB	PB
PB	Z	PS	PM	PB	PB	PB	PB

5.1. Optimization design variables

In order to search the optimum MFs in an attempt to reduce the fuel consumption and sustain the SoC level, MF points were selected as the optimization design variables. The MF points for the input and output spaces are shown in Fig. 5.

Among the fuzzy controller inputs, the SoC error was employed like Eq. (12) in Section 4. The SoC error is determined as the deviation from the SoC reference. Hence, the SoC reference affects the control performance of the fuzzy controller. Specifically, a trade-off problem exists in determination of the SoC reference value. This is because the high SoC reference induces an increment in fuel cell utilization and thus the stack is frequently operated in a low-efficiency region. Otherwise, battery utilization increases and the battery may be depleted during travel. Therefore, the SoC reference should be optimized for low fuel consumption and SoC maintenance.

Finally, the optimization design variables of the fuzzy controller are nine points ($o_{MF_{a1}}, o_{MF_{b1}}, o_{MF_{c1}}, o_{MF_{a2}}, o_{MF_{b2}}, o_{MF_{c2}}, o_{MF_{a3}}, o_{MF_{b3}}, o_{MF_{c3}}$) in MFs of the inputs and outputs, and the SoC reference (o_{SoCref}).

5.2. Genetic algorithm

The structure of a population in the GA is decided by the number of individuals (*nP*) and its genes (*nGene*). Each individual has the entire optimization design variables.

A fitness function should be designed considering the influence of the fuel consumption and the SoC deviation so as to find the optimum design variables of the fuzzy controller. In order to evaluate the fuel consumption of the FCHEV and then compare it with that of a conventional engine vehicle, an energy equivalent of the hydrogen usage was analyzed in terms of the gasoline litre equivalent per kilometer (GLEPK):

$$\mathrm{GLEPK} = \frac{\mathrm{LHV}_{H_2} \times \int_0^{t_F} W_{H_2}\,dt}{\mathrm{Distance}} \times \frac{100}{\mathrm{LHV}_{\mathrm{Gas}} \times \rho_{\mathrm{Gas}}}. \quad (13)$$

This measures how many litres of gasoline consumed for the equivalent energy of hydrogen for 100 km travel of the FCHEV. In addition, in order to prevent a large deviation between the final and the initial SoC, an absolute value of the SoC deviation was also considered as given by:

$$\left|\Delta \mathrm{SoC}\right| = \left|\mathrm{SoC_f} - \mathrm{SoC_0}\right|. \quad (14)$$

Finally, a fitness function was defined using following equation with normalization:

$$\mathrm{Fit} = \frac{1}{\alpha+\beta}\left[\alpha \times \frac{\mathrm{GLEPK}}{\mathrm{GLEPK_{target}}} + \beta \times \left(\frac{\left|\Delta \mathrm{SoC}\right|}{\left|\Delta \mathrm{SoC_{target}}\right|}\right)^2\right], \quad (15)$$

where $\mathrm{GLEPK_{target}}$ and $\Delta\mathrm{SOC_{target}}$ are minimal target values, $\alpha + \beta = 1$.

As observed in Eq. (15), the fitness function reflects the effect of the GLEPK and the SoC deviation.

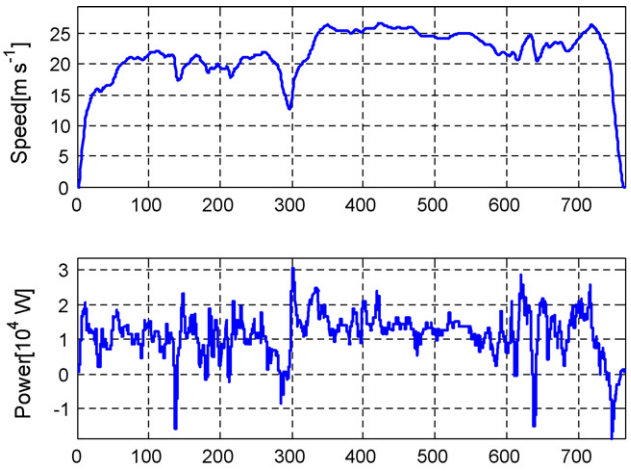

Fig. 6. The speed and required power profile of the HWFET.

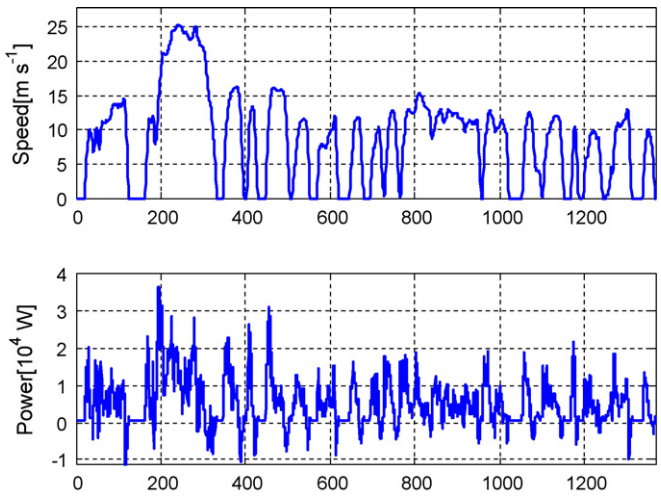

Fig. 7. The speed and required power profile of the UDDS.

6. Optimization using driving cycles

The design variables of the fuzzy controller have been optimized using the GA. The fitness function is evaluated through a driving cycle simulation of the respective individual generations and it offers criteria to determine an optimum set of design variables for the fuzzy controller. Therefore, the electric powertrain model of the FCHEV was implemented in SIMULINK® in order to perform the simulation for a given driving cycle.

6.1. Base driving cycles

Driving cycles can be sorted into two basic types: a highway driving cycle and a city driving cycle. In a highway driving, the idle time may be either short or zero and vehicle speed does not vary greatly. In city driving, an idle state frequently occurs while the vehicle is in use, and vehicle speed varies widely. Thus, discharge and charge operation of the battery can occur actively due to a rapid power demand and regenerative braking. Hence, when driving in cities, an increase in battery utilization through an aggressive charge and discharge operation can enhance fuel economy. Conversely, since quick power demand and aggressive battery operation rarely take place in highway driving, reduced battery utilization can help to lower fuel consumption and sustain battery SoC in suitable range.

Consequently, in this study, highway and city cycles were adopted as benchmarks so as to find the best sets of the optimization design variables. The two driving cycles employed were the highway federal emissions test (HWFET) for highway driving and the urban dynamometer driving schedule (UDDS) for city driving [35]. The UDDS cycle is also called U.S. FTP-72 (Federal Test Procedure) cycle or LA-4 cycle. The profiles of speed and required power for the two driving cycles shown in Figs. 6 and 7. The statistical features of each driving cycle are listed in Table 2 [36].

After driving cycle simulations for an individual in the population, the hydrogen consumption and the SoC deviation are evaluated. The hydrogen consumption is then converted to the GLEPK and miles per gallon of gasoline equivalent (MPGGE); MPGGE measures how many miles the FCHEV can travel on the equivalent energy of one gallon of gasoline. A MPGGE is calculated as follows:

$$\mathrm{MPGGE} = \frac{1}{(\mathrm{GLEPK}/100) \times \left[\frac{0.264172\,\mathrm{gal}}{1\,\mathrm{L}}\right] \times \left[\frac{1\,\mathrm{km}}{0.539612\,\mathrm{mile}}\right]}\ [\mathrm{mpg}]. \quad (16)$$

Table 2
Statistical features of selected driving cycles.

Driving cycle	UDDS	HWFET
Time [s]	1369	765
Distance [km]	11.99	16.51
Maximum speed [km h^{-1}]	91.25	96.4
Average running speed [km h^{-1}]	31.51	77.58
Average acceleration [m s^{-2}]	0.5	0.19
Average deceleration [m s^{-2}]	−0.58	−0.22
Idle time [s]	259	6

6.2. Baseline set of design variables

A baseline fuzzy controller was configured in order to present a criterion for a comparison of control performance. The design variables of the baseline are given in Table 3. The GA describes the evolution process which starts from the initial population. In this research, the baseline was used as an individual in the initial population of the GA process so as to obtain a better controller than the baseline set.

The MPGGEs were 56.38 and 48.18 mpg, respectively. For the HWFET cycle, the fuel consumption was lower than that of the UDDS cycle, because its operation stays in the high efficiency range, as can be seen in Fig. 8. In the UDDS cycle, on–off operation of the fuel cell stack system is frequently encountered and causes the fuel cell operation to fall into a lower efficiency range. In Fig. 8, the red dashed-line indicates the fuel cell efficiency when the fuel cell operates on steady-state. As seen, the fuel cell efficiency points were dispersed near the steady-state operation line.

Hence, in the UDDS cycle, the frequent on–off operation of the fuel cell should be prevented and the battery utilization has to rise

Table 3
Design variables of baseline.

G1	G2	G3	G4	G5	G6	G7	G8	G9	G10
$o_{\mathrm{MF}_{a1}}$	$o_{\mathrm{MF}_{b1}}$	$o_{\mathrm{MF}_{c1}}$	$o_{\mathrm{MF}_{a2}}$	$o_{\mathrm{MF}_{b2}}$	$o_{\mathrm{MF}_{c2}}$	$o_{\mathrm{MF}_{a3}}$	$o_{\mathrm{MF}_{b3}}$	$o_{\mathrm{MF}_{c3}}$	o_{SoCref}
10	20	45	0.15	0.3	0.45	3	10	15	0.5

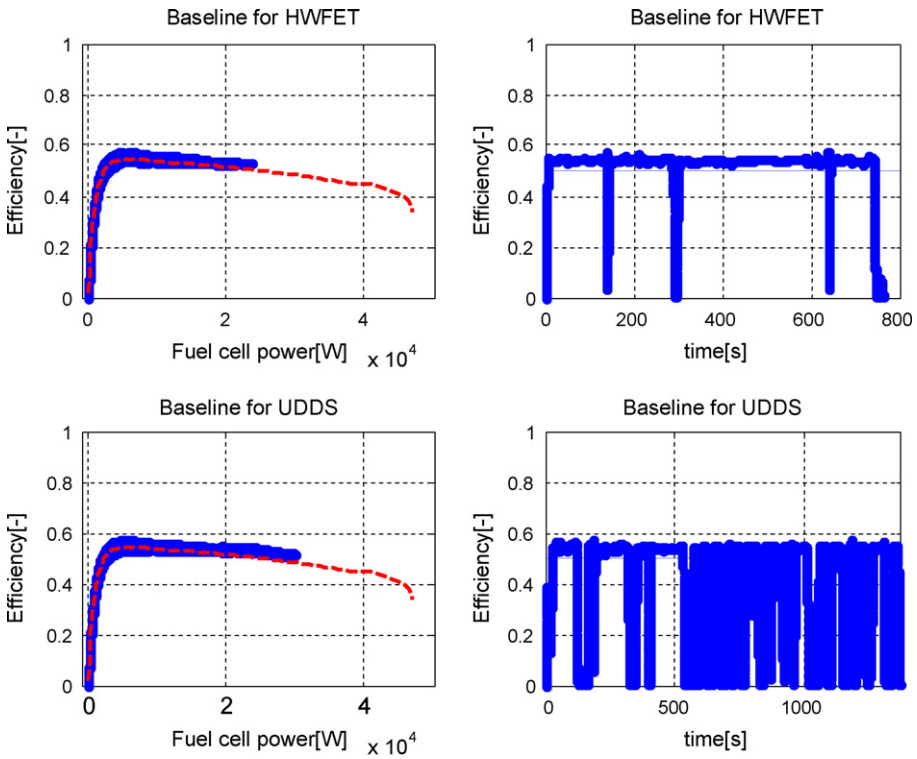

Fig. 8. The fuel cell stack efficiency of the baseline for two cycles.

Table 4
Target values in fitness function.

	Target MPGGE [mpg] (GLEPK [L/100 km])	Target $\|\Delta SoC\|$ [%]
HWFET	59.20 (3.44)	1.5
UDDS	50.59 (4.03)	1.5

through the aggressive operation of charge and discharge by the battery, in order to attain enhanced fuel economy. By performing optimization of the design variables, it is possible to design the power distribution controller, which follows the above description for the optimum power management according to base driving cycles.

6.3. Optimization results

The target values in the fitness function (see Eq. (15)) were chosen as shown in Table 4. The target value of fuel consumption was determined at 5% enhancement with respect to the MPGGE of the baseline set, depending on each driving cycles. The deviation between the initial and the final SoC ($|\Delta SoC|$) was limited to 1.5%; this target value was applied Kim and Peng [17]. Since it is important to maintain the battery SoC within a suitable range with respect to the power management of a hybrid vehicle [17], α and β are chosen as 0.2 and 0.8, respectively.

The GA optimization results for two driving cycles are given in Table 5. The optimized set attains the enhanced MPGGEs, which are more than 5% higher than the baseline set, as reported in Table 6. In addition, although the baseline violates the target value of $|\Delta SoC|$ ($|\Delta SoC| < 1.5\%$), the SoC maintenance problem site is well regulated ($|\Delta SoC| \leq 0.09\%$) when the optimized set is used. The data in Fig. 9 illustrate that the optimized set can prevent the frequent on–off operation of the fuel cell at the early stage of the design phase. Thus, the optimized sets can accomplish lower fuel consumption and the SoC maintenance. Furthermore, in Fig. 10, it is shown that the optimized set for the UDDS cycle induces a larger standard deviation in battery power and SoC than those in the HWFET cycle. From this result, it is verified that a more aggressive operation (charge and discharge) of the battery is accomplished with the UDDS cycle.

Table 5
Optimized set for HWFET and UDDS cycles.

	G1	G2	G3	G4	G5	G6	G7	G8	G9	G10
HWFET	21.41	46.54	84.96	0.08	0.14	0.41	7.44	17.76	24.80	0.56
UDDS	20.55	53.48	79.72	0.04	0.33	0.45	1.23	6.59	30.47	0.60

Table 6
MPGGE comparison of baseline and optimized sets.

	MPGGE [mpg]			SoC [%]	
	Baseline set	Optimized set	Enhancement [%]	Baseline set	Optimized set
HWFET	56.38	59.34	5.25	4.13	0.01
UDDS	48.18	51.56	7.02	2.17	0.09

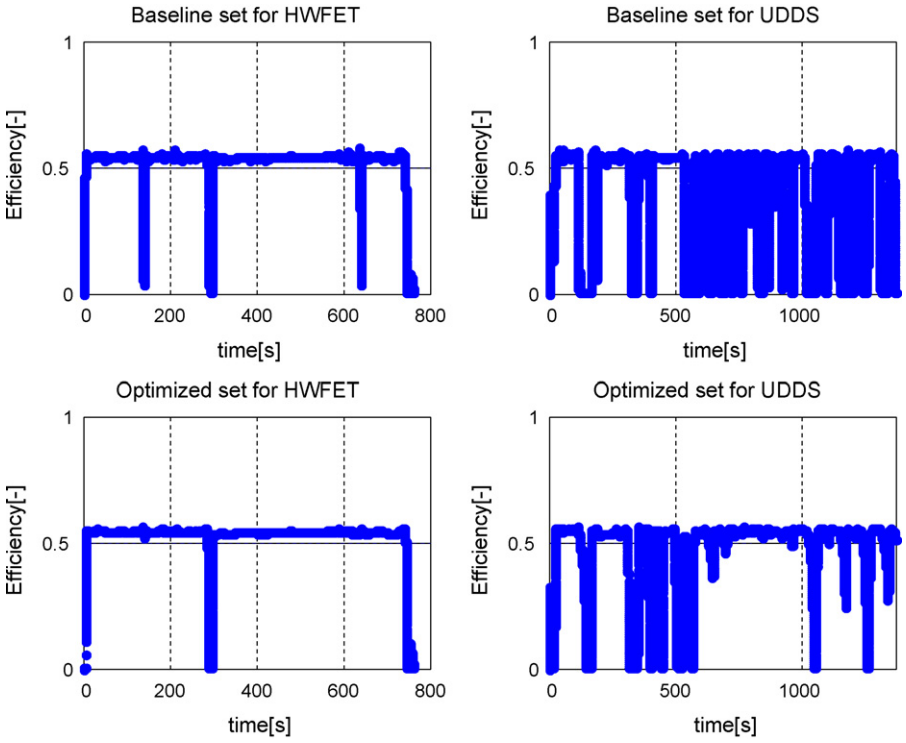

Fig. 9. The efficiency of fuel cell stacks for the baseline set and the optimized set.

7. Stochastic fuzzy controller (SFC)

7.1. Adaptive membership functions of SFC

The adaptive membership function is a key component of the SFC to distribute power optimally between a fuel cell and a battery in the FCHEV. Its operation concept is very simple. The transformation of the MFs in the SFC is illustrated in Fig. 11; the MFs can be changed depending on the probability $p(t)$. The probability represents the current driving pattern. Specifically, if the probability becomes close to one, this means that a current driving pattern has the characteristics of urban driving. Conversely, if the probability approaches zero, the driving pattern has the characteristics of highway driving. Finally, the adaptive MFs (MF_{SFC}) are determined using a convex combination which is a linear combination of two points. These two points (MF_{HWFET} and MF_{UDDS}) are provided by the two optimized sets for the highway and urban driving cycles. The following equation calculates the movement of the adjusted MF points of the SFC:

$$MF_{SFC} = MF_{UDDS} \times p(t) + MF_{HWFET} \times (1 - p(t)). \quad (17)$$

As seen, MF_{SFC} becomes near to MF_{UDDS} as $p(t)$ approaches one; otherwise, MF_{SFC} comes close to MF_{HWFET}. Specifically, the MFs can be transformed to follow the optimized MF set according to a current driving pattern. Therefore, the performance of the SFC is directly affected by how exactly the probability recognizes a current driving pattern. Accordingly, the probability is a key factor of the SFC to achieve the optimum power distribution between the two power sources.

7.2. Probability evaluation

In order to recognize driving patterns accurately, a probability evaluation method, which uses statistical data for the required power, is proposed in this section. In the city driving cycle, since the variation of vehicle speed is large and rapid, the variation of the required power is also wide. Conversely, in the highway cycle, the speed variation is small and slow; thus, the required power does not change greatly. Therefore, the dispersion of the required power may offer statistical information that can be helpful in characterizing driving patterns. In this study, a standard deviation is used and is a measure of the dispersion of collected values. A useful property of standard deviation is that, unlike variance, it is expressed in the

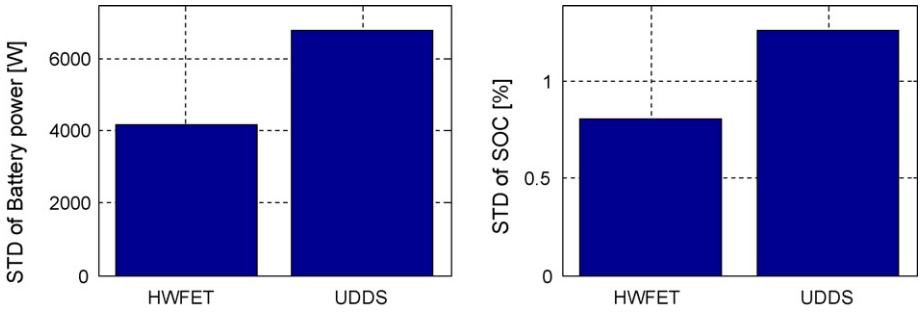

Fig. 10. The comparison results of optimized sets for each driving cycle.

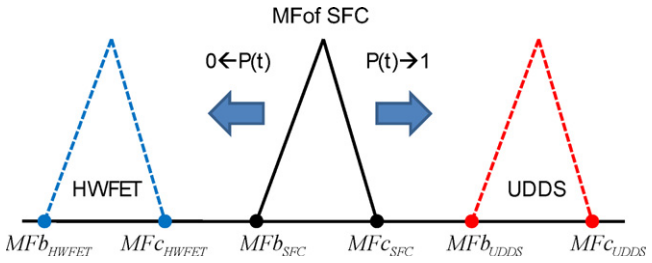

Fig. 11. Adaptive membership function of the SFC.

same units as the data. Fig. 12 includes average value (Mean Power) and standard deviation (STD) of the required power for the HWFET and UDDS cycles.

The standard deviation of the UDDS cycle is higher than that of the HWFET but its difference is very small. On the other hand, the ratio of the standard deviation to the average value in the UDDS cycle is larger than that in the HWFET cycle. For actual driving, the evaluation of the power variation should be considered to be the ratio of standard deviation to average power. If the standard deviations are similar to each other and the difference of each average power is much larger, then the effect of the power variation which has a low average power should be regarded as large and severe. Hence, in this study, the ratio of standard deviation to average power was applied to evaluate the probability.

Since it is impossible to obtain the standard deviation and the average of the required power as prior-knowledge before running the vehicle, these values have to be calculated in real-time while driving. Accordingly, they can be predicted by using values from data collected for a given time period. In other words, a moving standard deviation and moving average were used in this study. They are referred as a statistical technique used to analyze a set of data points by creating a standard deviation and an average for one subset of the full data set at a time. They are computed as follows:

$$P_{\text{req}}^{t_1} = \left[P_{\text{req}}^1 P_{\text{req}}^2 P_{\text{req}}^3 \cdots P_{\text{req}}^N\right], P_{\text{req}}^{t_2} = \left[P_{\text{req}}^2 P_{\text{req}}^3 \cdots P_{\text{req}}^N P_{\text{req}}^{N+1}\right],$$
$$P_{\text{mov}}^{t_1,\text{avg}} = \frac{\text{sum}(P_{\text{req}}^{t_1})}{N}, P_{\text{mov}}^{t_1,\text{STD}} = \left(\frac{\sum_1^N (P_{\text{req}}^N - P_{\text{mov}}^{t_1,\text{avg}})}{N}\right)^{1/2}, \quad (18)$$
$$P_{\text{mov}}^{t_2,\text{avg}} = \frac{\text{sum}(P_{\text{req}}^{t_2})}{N}, P_{\text{mov}}^{t_2,\text{STD}} = \left(\frac{\sum_2^{N+1} (P_{\text{req}}^N - P_{\text{mov}}^{t_2,\text{avg}})}{N}\right)^{1/2}.$$

Finally, the probability is evaluated as:

$$p(t) = \begin{cases} 1, & \text{if} \dfrac{P_{\text{mov}}^{t,\text{STD}}}{P_{\text{mov}}^{t,\text{avg}}} > 1, \\ \dfrac{P_{\text{mov}}^{t,\text{STD}}}{P_{\text{mov}}^{t,\text{avg}}}, & \text{if } 0 \le \dfrac{P_{\text{mov}}^{t,\text{STD}}}{P_{\text{mov}}^{t,\text{avg}}} \le 1, \\ 0, & \text{if } \dfrac{P_{\text{mov}}^{t,\text{STD}}}{P_{\text{mov}}^{t,\text{avg}}} < 0. \end{cases} \quad (19)$$

In this probability, the tuning parameters are a sampling period and a time-horizon, which define a time-period for data collection and time-length for calculating statistics, respectively. Since the change of the required power is dependent on the driver's acceleration pedal input and its variation is not too large or fast, the sampling period can be determined easily. Typically, the vehicle speed data for driving cycles are collected every 1 s and thus the sampling period was chosen to 0.1 s in this study.

In order to choose an appropriate time-horizon, it is necessary to analyze the effects of the time-horizon on the response of the probability evaluation. The longer the period of the time-horizon, the slower is the driving pattern recognition. By contrast if the time-horizon is too short, it is hard to recognize a driving pattern adequately between highway driving and urban driving. This is due to the fact that the variation of the moving average is rapid and large regardless of a driving pattern. The problem becomes more severe for the UDDS as shown in Fig. 13. The

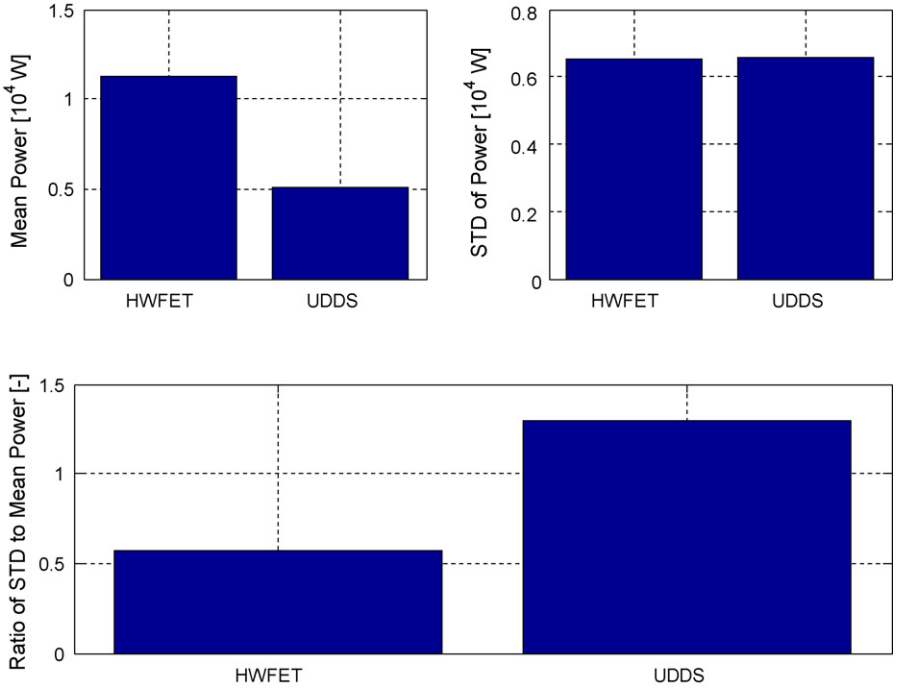

Fig. 12. The average and the standard deviation of the required power for the HWFET and the UDDS.

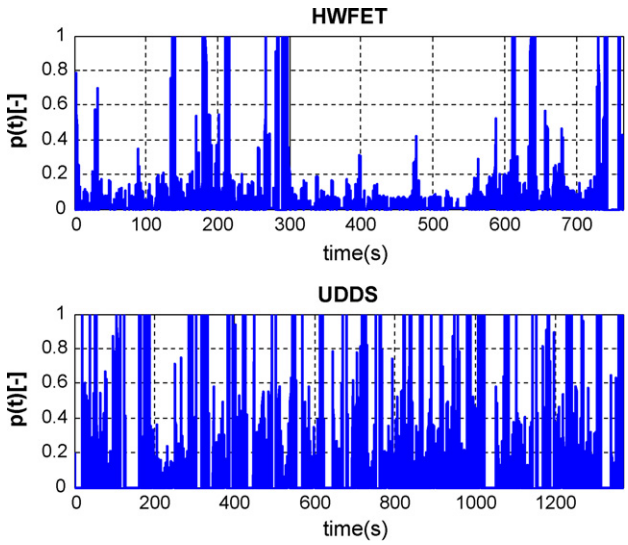

Fig. 13. The analysis results of the HWFET cycle and the UDDS cycle for short time-horizon.

results of well-tuned parameters are described in Fig. 14. The time-horizon was 60 s and the probability was refreshed every 0.1 s in accordance with the sampling period. As can be seen in Fig. 14, a serious rapid change of the probability does not appear and it reflects individual characteristics of own driving cycle. These tuning results of the probability evaluation can be simply obtained through an analysis of the required power data. Therefore, it is fast and easy.

In signal processing, cross-correlation is a measure of the similarity of two waveforms as a function of a time-lag applied to one of them. A cross-correlation between the probabilities of the two driving cycles is 0.8462 at zero lag time. This indicates that the probabilities are very similar each other. Therefore, the probability evaluation should be modified in order to distinguish clearly the two driving cycles. In this research, the probability is revised using

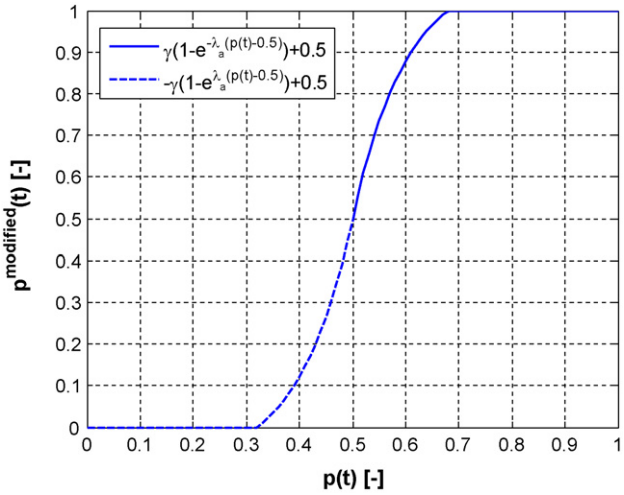

Fig. 15. The revision function for the probability.

following function:

$$p'(t) = \begin{bmatrix} \gamma(1 - e^{-\lambda_a(p(t)-0.5)}) + 0.5 & \text{if} \quad p(t) \geq 0.5 \\ -\gamma(1 - e^{\lambda_a(p(t)-0.5)}) + 0.5 & \text{if} \quad p(t) < 0.5 \end{bmatrix},$$

$$p^{\text{modified}}(t) = \begin{bmatrix} 1 & \text{if} \quad p'(t) > 1 \\ p'(t) & \text{if} \quad 0 \leq p'(t) \leq 1 \\ 0 & \text{if} \quad p'(t) < 0 \end{bmatrix}. \tag{20}$$

The revision function is shown graphically in Fig. 15. The respective modified probabilities are obtained as shown in Fig. 16. Using these modified probabilities, the cross-correlation is calculated again. The cross-correlation is very low i.e., 0.2029, at zero lag time. Thus, the modified probability can provide more exact information on a given driving cycle.

Since there are many driving cycles specific to a particular location, society and county, more simulations are needed to investigate further the performance of power control strategies. In this study, an additional two driving cycles were chosen, namely, the Unified Cycle Driving Schedule (UCDS) and the New European Driving Cycle (NEDC). The cross-correlation between the four driving cycles is given in Table 7. The UCDS cycle and NEDC cycle are urban driving cycles because they have a high correlation with the UDDS

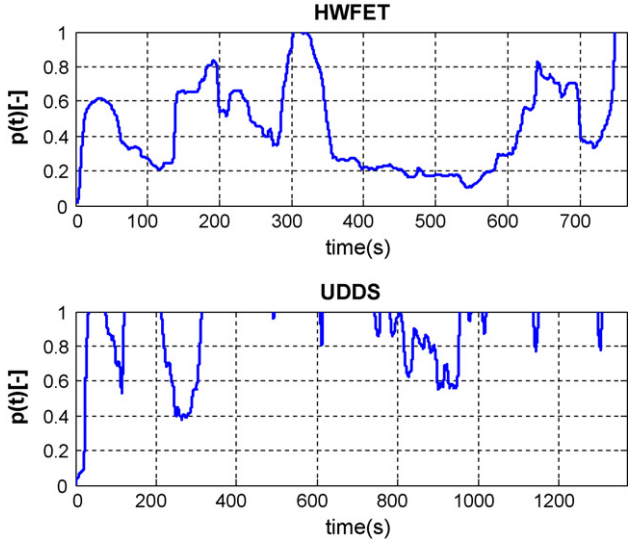

Fig. 14. The analysis results of the two cycles for 60 s time-horizon.

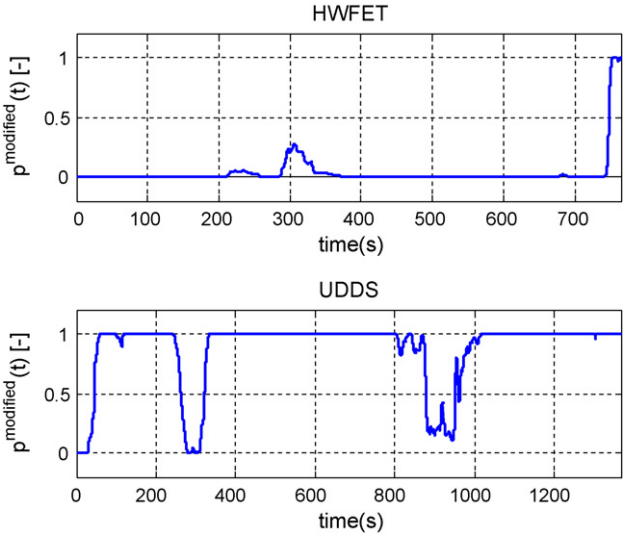

Fig. 16. The modified probabilities for two driving cycles.

Table 7
Test cases of off-line simulations.

	HWFET-UCDS	HWFET-NEDC	UDDS-UCDS	UDDS-NEDC
Correlation	0.2732	0.2568	0.9179	0.8613

cycle, as reported in Table 7.

8. Results of off-line simulation and hardware-in-the-loop simulation (HILS)

This section presents the results of simulation studies and HILS tests to validate the performance of the SFC for power distribution in a FCHEV. Compared with the baseline set and the optimized fuzzy controllers, the performance of the SFC is verified for the four diving cycles: HWFET, UDDS, UCDS, NEDC. As mentioned above in Section 1, the power distribution between two power sources is an important factor for minimum fuel consumption and maintenance of battery SoC. Accordingly, the performance of each controller should be evaluated in terms of the MPGGE and the SoC deviation ($|\Delta SoC|$). Therefore, the MPGGE and $|\Delta SoC|$ provide criteria for choosing the best controller. Finally, the best power control strategy is implemented on a real electronic control unit (ECU), which is then tested using a HILS environment in order to check a realization problem of the power control strategy and verify its performance in the real world. Test cases for the off-line simulation are given in Table 8.

8.1. Off-line simulation results

8.1.1. Results for HWFET cycle

The MPGGEs and $|\Delta SoC|$ for the HWFET cycle are reported in Table 9. The information that the SFC has the maximum MPGGE which is similar to the value of the HWFET OPT. The MPGGE of the UDDS OPT, however, is lower than those of the HWFET OPT and the SFC. As can also be seen in Table 9, BASE and UDDS OPT violate the $|\Delta SoC|$ target value ($|\Delta SoC| < 1.5\%$). On the contrary, the SoC maintenance problem is well regulated ($|\Delta SoC| \leq 1.09\%$) when the HWFET OPT or the SFC is used.

The simulation results of the SFC show that the SFC can transform its own MFs to the optimized set according to the current driving pattern. On the other hand, the performance of the UDDS OPT is not satisfactory in terms of fuel consumption and SoC deviation. This is due to fact that the UDDS OPT is a controller optimized for the UDDS cycle. Therefore, this result indicates that a controller optimized using a specific driving cycle is not applicable to the other cycles.

8.1.2. Results for UDDS cycle

For the UDDS cycle, the results of the MPGGEs and $|\Delta SoC|$ are presented in Table 10. The HWFET OPT has the largest MPGGE and the UDDS OPT is ranked second. The HWFET OPT, however, is not suitable for optimum power control strategies because the $|\Delta SoC|$ target value (1.5%) is violated. Therefore, the best controller for the UDDS cycle is the UDDS OPT, which is followed by the SFC.

The SFC has a MPGGE that is close to, or higher than, that of the optimized set for the two driving cycles (see Tables 9 and 10) as the intended results at early stage of design phase. In addition, the $|\Delta SoC|$ of the SFC is maintained within the target value. Hence, the proposed probability evaluation is found to be suitable for the recognition of a driving pattern and stochastic approaches to the power control of the FCHEV.

Table 9
MPGGEs and $|\Delta SoC|$ for HWFET cycle.

	BASE	HWFET OPT	UDDS OPT	SFC
MPGGE	56.38	59.35	57.09	59.96
Ranking	-	2*	-	1*
$\|\Delta SoC\|$ [%]	4.13	0.01	4.80	1.09
Constraint	X	O	X	O
Max ΔSoC [%]	4.23	0.11	4.80	0.13
Min ΔSoC [%]	−0.59	−3.77	−2.29	−3.35

(*) Means higher ranks than third position. (-) Means that $|\Delta SoC|$ is larger than target value 1.5%. If $|\Delta SoC| < 0.015$ (1.5%), than O, else X.

Table 10
MPGGEs and $|\Delta SoC|$ for UDDS cycle.

	BASE	HWFET OPT	UDDS OPT	SFC
MPGGE	48.18	52.61	51.56	51.42
Ranking	-	-	1*	2*
$\|\Delta SoC\|$ [%]	2.17	2.71	0.09	0.11
Constraint	X	X	O	O
Max ΔSoC [%]	15.63	0.06	2.81	3.29
Min ΔSoC [%]	−0.49	−3.79	−1.82	−3.15

(*) Means higher ranks than third position. (-) Means that $|\Delta SoC|$ is larger than target value 1.5%. If $|\Delta SoC| < 0.015$ (1.5%), than O, else X.

The MPGGE values for the driving cycle optimized sets (HWFET OPT, UDDS OPT) in Tables 9 and 10 indicate that the optimized sets reveal mutually exclusive results for the driving cycles. In other words, for the HWFET cycle, the fuzzy controller which adopts the UDDS OPT induces a much lower MPGGE than the HWFET OPT. For the UDDS cycle, although the HWFET OPT has a higher MPGGE than the other optimized set, it cannot satisfy the $|\Delta SoC|$ target value. Therefore, these simulation outcomes demonstrate that only one optimization result is unable to guarantee the optimum performance despite a change in cycle.

8.1.3. Results for UCDS cycle

The California Unified Cycle (UC) is a dynamometer driving schedule for light-duty vehicles that has been developed by the California Air Resources Board. The test is also referred to as the UCDS [37]. The properties of the UCDS cycle, such as vehicle speed, required power and probability are shown in Fig. 17. The statistical features of the UDDS are given in and the Table 11. UCDS. The UCDS cycle has a long idle time and an average acceleration that is high, as found with the UDDS. In addition, the probability and the cross-correlation (see Fig. 17 and Table 7) also show that the UCDS cycle is an urban driving mode. Therefore, the simulation is executed using the test case for the UDDS in Table 8.

The MPGGE results for the two optimized sets (see Table 12) show that the optimized set (UDDS OPT) for the corresponding driving cycle has a lower MPGGE than the HWFET OPT does. The HWFET OPT, however, cannot meet the $|\Delta SoC|$ target value and is thus not suitable as a power control strategy. In summary, the best power control strategy is the SFC.

Table 8
Cross-correlation for four driving cycles.

	Fuzzy controllers			
	1	2	3	4
HWFET	Baseline set	Optimized set for HWFET	Optimized set for UDDS	SFC
UDDS	Baseline set	Optimized set for HWFET	Optimized set for UDDS	SFC
Abbreviations	BASE	HWFET OPT	UDDS OPT	SFC

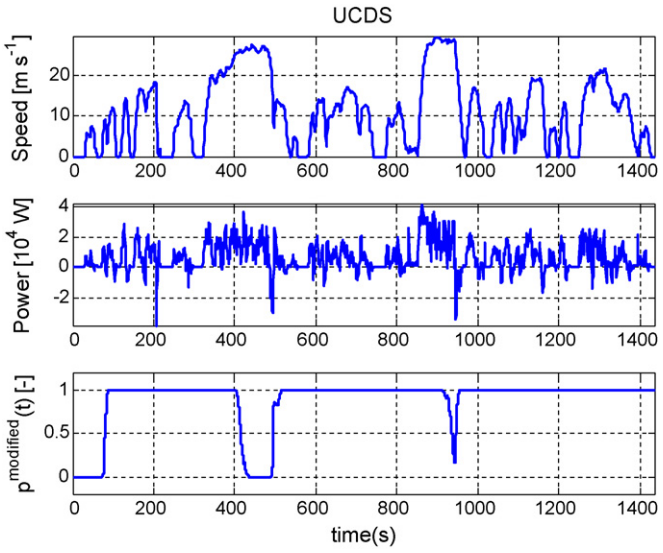

Fig. 17. The speed, required power profile and probability of the UCDS.

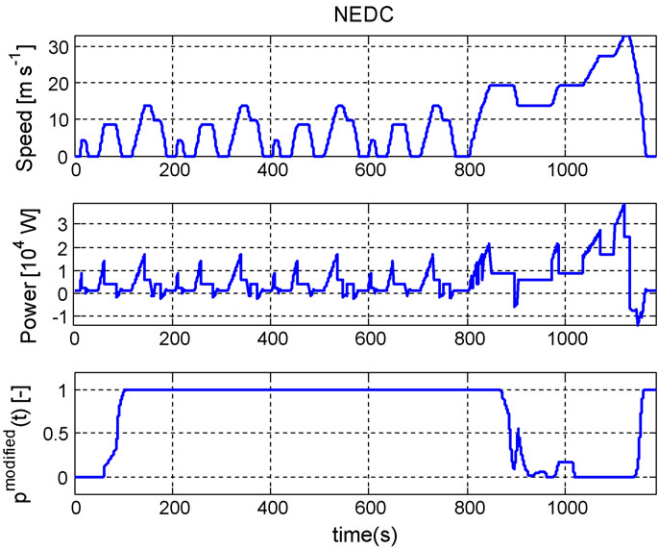

Fig. 18. The speed, required power profile and probability of the NEDC.

8.1.4. Results for NEDC cycle

The NEDC is a driving cycle that consists of four repeated ECE (Economic commission for Europe) driving cycles and an Extra-Urban driving cycle, or EUDC [38]. The properties of the NEDC cycle are presented in Fig. 18. As shown in Table 11, the NEDC cycle also has a long idle time and the average acceleration is high, as for the UDDS. In addition, the probability and the cross-correlation (see Fig. 18 and Table 7) also show that the NEDC cycle is an urban driving mode. Therefore, the simulation is performed using the test case for the UDDS in Table 8.

From the MPGGE results of the two optimized sets (see Table 13), it is found that the optimized set (UDDS OPT) for the corresponding driving cycle has a lower MPGGE than the HWFET OPT. This is because the NEDC cycle is not a complete city cycle like the UDDS cycle, but a mixed cycle that has the characteristics of a highway cycle and an urban cycle. This is demonstrated by the fact that the probability shows the characteristics of a highway cycle for the last 400 s, as can be seen in Fig. 18; therefore, the probability is much lower than one after approximately 800 s. Thus, since the SFC can estimate a current driving pattern successfully and transform the MFs effectively, it achieves a higher MPGGE than the UDDS OPT and maintains |ΔSoC| within the target value. Fig. 19 describes the trajectories of the fuel cell power and the battery power. The fuel cell power of the SFC follows a trajectory that is connected to each corresponding driving pattern. The fuel cell power of the SFC in the initial 800 s time section is very similar to the result for the UDDS OPT, but is very close to the trajectory of the HWFET OPT for the last

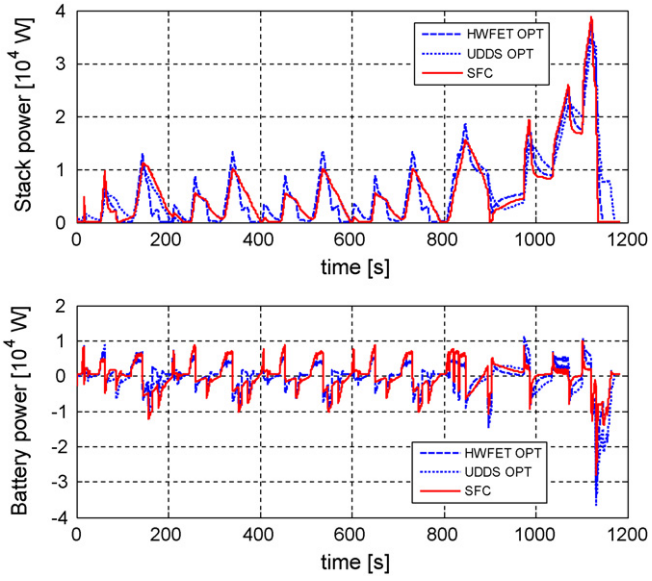

Fig. 19. Comparison of the fuel cell and battery power trajectory for the NEDC.

Table 11
Statistical features of UDDS, UCDS and NEDC cycles.

Driving cycle	UDDS	UCDS	NEDC
Time [s]	1369	1435	1184
Distance [km]	11.99	15.8	10.93
Maximum speed [km h^{-1}]	91.25	108.15	120
Average running speed [km h^{-1}]	31.51	39.6	33.21
Average acceleration [m s^{-2}]	0.5	0.67	0.54
Average deceleration [m s^{-2}]	−0.58	−0.75	−0.79
Idle time [s]	259	234	298

Table 12
MPGGEs and |ΔSoC| for UCDS cycle.

	BASE	HWFET OPT	UDDS OPT	SFC
MPGGE	45.96	49.87	48.57	49.23
Ranking	-	-	2*	1*
|ΔSoC| [%]	10.55	1.73	0.88	0.88
Constraint	X	X	O	O
Max ΔSoC [%]	13.33	1.28	8.53	2.53
Min ΔSoC [%]	−0.38	−3.77	−2.66	−2.88

(*) Means higher ranks than third position. (-) Means that |ΔSoC| is larger than target value 1.5%. If |ΔSoC| < 0.015 (1.5%), than O, else X.

Table 13
MPGGEs and |ΔSoC| for NEDC cycle.

	BASE	HWFET OPT	UDDS OPT	SFC
MPGGE	48.69	50.33	48.21	50.75
Ranking	-	2*	-	1*
|ΔSoC| [%]	4.45	1.04	5.28	0.49
Constraint	X	O	X	O
Max ΔSoC [%]	4.67	1.25	5.41	1.66
Min ΔSoC [%]	−0.76	−5.07	−3.91	−3.72

(*) Means higher ranks than third position. (-) Means that |ΔSoC| is larger than target value 1.5%. If |ΔSoC| < 0.015 (1.5%), than O, else X.

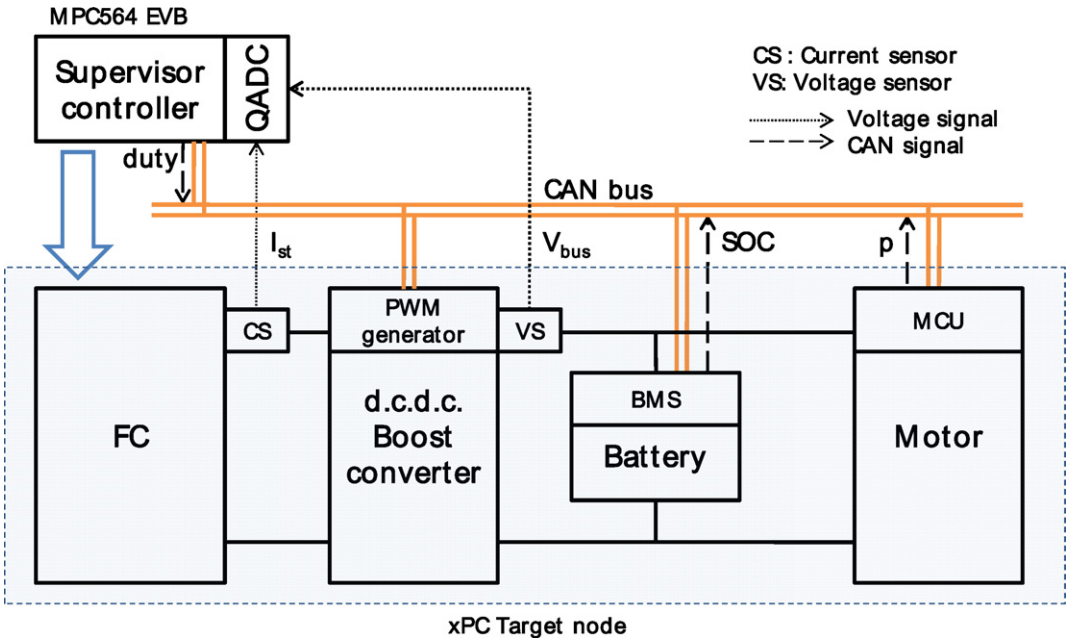

Fig. 20. The network-based power management system of the FCHEV.

400 s. The same trends are observed for the trajectories of battery power.

From the results of the four diving cycles, it is verified that the best power control strategy is the SFC. Thus the SFC will be implemented on a real ECU in order to test the feasibility of the control algorithm in real-time application.

8.2. HILS test

The physical configuration of a HILS environment is composed of a command station and a target node. In the command station, an engineer designs a mathematical model and runs its off-line simulations. Furthermore, a HILS model for a real-time simulation is also generated at this station. In the target node, the HILS model is transferred from the command station so that the real-time simulation of the HILS model can be executed. In this study, a MPC564EVB, which is a MPC564®-based evaluation board [39], was employed as an ECU for developing the SFC in a real application. The xPC Target solution of MATLAB®/SIMULINK® [40] served as the target node.

8.2.1. Network-based power management system of FCHEV

In this study, it is assumed that several controllers are integrated using a network and thus, controllers can exchange information for the optimum power management of a FCHEV by using the network bus. When a control system is networked, it can not only share mutual data, but also extend its functionalities throughout the modulation of the control system [41]. A schematic diagram of the FCHEV's network-based control system developed in this study and signal flow is given in Fig. 20. The controller area network (CAN) protocol was applied as a network protocol [42].

The network-based power management system of the FCHEV is configured with a supervisor controller, a battery management system (BMS) and a motor control unit (MCU). The supervisor controller conducts not only the power management, but also serves as a fuel cell controller. Therefore, the stochastic fuzzy control algorithm is embedded in the supervisor controller. The SFC requires four inputs: the stack current, the bus voltage, the battery SoC and the probability. Its output is the duty ratio. The stack current and the bus voltage are measured using queued analog-to-digital converter (QADC) modules in MPC564® and the battery SoC value is received from the BMS using the CAN bus. Finally, the duty ratio is transferred to a PWM generator via the network; the PWM generator is a smart actuator [41] and is able to operate independently as it is installed in the d.c.–d.c. converter. In this study, the PWM generator is implemented virtually in the target node and simulated in real-time.

The BMS checks and manages battery states, such as temperature and current flow. In addition, the BMS estimates the SoC level of the battery and sends the value to the supervisor controller through the network. It also virtually operates in the target node. The MCU plays controls motor torque and speed in order to meet the power demand of drivers. It is assumed that a motor can be perfectly controlled by the MCU, and it is analyzed as a current source in this research. The MCU also monitors the motor power consumed for a certain period and calculates its moving average and standard deviation. Then, the probability is calculated and transmitted to the supervisor controller via the CAN bus. Consequently, the supervisor controller is only a real ECU, with the others operate virtually in the target node. The stochastic fuzzy control algorithm is embedded in the supervisor controller.

8.3. Results of HILS test

The HILS test of the SFC was conducted for the four driving cycles in order to confirm that the proposed power control strategy would be available for practical power distribution in FCHEVs.

The HILS test gives very similar results for the duty, fuel cell power, battery power, and SoC. Thus, the MPGGE has an almost identical value to that for the off-line simulation; the errors with respect to the off-line simulation value are given in Table 14. These small errors between the off-line simulation and the HILS results are induced by data loss, which can occur during two signal conversion processes: digital-to-analog conversion in the target node and analog-to-digital conversion in the ECU. Finally, the HILS results indicate that the SFC is suitable for a real application.

Table 14
HILS results of SFC for four driving cycles.

MPGGE [mpg]	HWFET	UDDS	UCDS	NEDC
Off-line simulation	59.96	51.42	49.23	50.75
HILS	60.006	51.535	49.310	50.828
Error [%]	0.0834	0.2331	0.1622	0.1571

9. Summary and concluding remarks

The FCHEV is a prospective vehicle to solve global energy supply and environmental problems. Significant investment is needed, however, to develop a commercial FCHEV. In particular, power management of the power sources is extremely challenging. Therefore, this study has proposed a novel power control strategy for minimizing fuel consumption and maintaining battery SoC.

A the dynamic state–space model of the electric powertrain in a parallel-type FCHEV has been developed using an equivalent circuit model of the electric powertrain, which consists of a fuel cell stack system, a d.c.–d.c. converter, and a battery. It is possible to observe the dynamic behaviour of the fuel cell current and the bus voltage. Using this model, a fuzzy controller is proposed the power management of the FCHEV. Furthermore, a new method to prevent oxygen starvation in the fuel cell has been formulated and implemented in the fuzzy controller. It is optimized by using a generic algorithm to achieve the maximum MPGGE and the SoC maintenance for two driving cycles. The optimized fuzzy controller can achieve MPGGE enhancement, i.e., 5.25% and 7.02% for the HWFET cycle and the UDDS cycle respectively, while meeting the $|\Delta SoC|$ target value ($|\Delta SoC| < 1.5\%$).

Several power control strategies are proposed for the optimum power control of the FCHEV, e.g., DP, SDP, ECMS, and optimized fuzzy control with a GA. These strategies have a common problem in that it is not possible to always guarantee optimum performance for different driving cycles. Hence, the SFC is developed to achieve optimum results through a stochastic approach, even though the driving cycle may change. In addition, an evaluation method of the probability for driving pattern recognition is devised using the information of the required power, which can be obtained during travel. The controller has been tested for four driving cycles, namely HWFET, UDDS, UCDS, and NEDC.

Finally, through off-line simulation and the HILS test, it has been verified that the SFC with the proposed probability can not only be implemented in a real ECU, but also can attain minimum fuel consumption and SoC maintenance in a real-world application.

Acknowledgements

This research was financially supported by the Ministry of Knowledge Economy (MKE) and the Korea Institute for Advancement in Technology (KIAT) through the Workforce Development Program in Strategic Technology.

References

[1] C.C. Lin, J.M. Kang, J.W. Grizzle, H. Peng, Proc. Am. Control Conf. 4 (2001) 2878–2883.
[2] S.D. Knights, K.M. Colbow, J. St-Pierre, D.P. Wilkinson, J. Power Sources 127 (2004) 127–134.
[3] O. Erdinc, B. Vural, M. Uzunoglu, Y. Ates, Int. J. Hydrogen Energy 34 (2008) 5223–5233.
[4] N. Jalil, N.A. Kheir, M. Salman, Proc. Am. Control Conf. 1 (1997) 689–693.
[5] H.Y. Cho, W. Gao, H.L. Ginn, IEEE Power Electron. (2004) 159–166.
[6] D.D. Boettner, G. Paganelli, Y.G. Guezennec, G. Rizzoni, M.J. Moran, J. Energy Resour. ASME 124 (2002) 20–27.
[7] K. Wipke, T. Markel, D. Nelson, EVS 18 (2001).
[8] M. Salman, N.J. Schouten, N.A. Kheir, Proc. Am. Control Conf. 1 (2000) 524–528.
[9] B.M. Baumann, G. Washington, B.C. Glenn, G. Rizzoni, IEEE-ASME T. Mech. 5 (2000) 58–72.
[10] N.J. Schouten, M.A. Salman, N.A. Kheir, Control Eng. Pract. 11 (2003) 171–177.
[11] J. Won, R. Langari, IEEE Trans. Veh. Technol. 54 (2005) 925–934.
[12] J. Won, R. Langari, IEEE Trans. Veh. Technol. 54 (2005) 935–953.
[13] M.H. Hajimiri, F.R. Salmasi, ICEHV'06 (2006) 1–5.
[14] D. Gao, Z. Jin, Q. Lu, J. Power Sources 185 (2008) 311–317.
[15] C.C. Lin, H. Peng, J.W. Grizzle, Proc. Am. Control Conf. 5 (2004) 4710–4715.
[16] C.C. Lin, M.J. Kim, H. Peng, J. Dyn. Syst. Trans. ASME 128 (2006) 878–890.
[17] M.J. Kim, H. Peng, J. Power Sources 165 (2007) 819–832.
[18] A. Sciarretta, M. Back, L. Guzzella, IEEE Trans. Control Syst. Technol. 12 (2004) 352–363.
[19] P. Rodatz, G. Paganelli, A. Sciarretta, L. Guzzella, Control Eng. Pract. 13 (2005) 41–53.
[20] A. Wang, W. Yang, WCICA 2006 2 (2006) 8324–8328.
[21] A. Wang, W. Yang, WCICA 2006 2 (2006) 8329–8333.
[22] A. Poursamad, M. Montazeri, Control Eng. Pract. 16 (2008) 861–873.
[23] M. Uzunoglu, M.S. Alam, Energy Convers. Manage. 48 (2007) 1544–1553.
[24] N. Mohan, T.M. Undeland, W.P. Robbins, Power Electronics, third ed., John-Wiley, 2003.
[25] Y. Haitao, Z. Yulan, S. Zechang, W. Gang, J. Power Sources 180 (2008) 821–829.
[26] J. Ryu, K. Noh, J. Kim, H. Kim, KSAE 7 (1999) 105–111.
[27] W. Lee, M. Yoon, M. Sunwoo, Proc. Inst. Mech. Eng. D: J. Aut. Eng. 217 (2002) 41–52.
[28] J.T. Pukrushpan, H. Peng, A.G. Stefanopoulou, J. Dyn. Syst. Trans. ASME 126 (2004) 14–25.
[29] A.Z. Weber, J. Newman, J. Electrochem. Soc. 150 (2003) 1008–1015.
[30] T.A. Zawodzinski, C. Derouin, S. Radzinski, R.J. Sherman, V.T. Smith, T.E. Springer, S. Gottesfeld, J. Electrochem. Soc. 140 (1993) 1041–1047.
[31] H.S. Ramirez, R.S. Ortigoza, Control Design Techniques in Power Electronics Devices, Springer, 2006.
[32] V.H. Johnson, J. Power Sources 110 (2002) 321–329.
[33] J.M. Andújar, F. Segura, M.J. Vasallo, Renew. Energy 33 (2008) 813–826.
[34] L. Wang, A course in fuzzy systems and control, Prentice-Hall International, Inc., 1997.
[35] Website of United States Environment Protection Agency (EPA) http://www.epa.gov/nvfel/testing/dynamometer.htm.
[36] ADVISOR 2002 (ADvanced VehIcle SimulatOR) developed by the Nation Renewable Energy Laboratory (NREL), 2002.
[37] http://www.dieselnet.com/standards/cycles/uc.html.
[38] http://www.dieselnet.com/standards/cycles/ece_eudc.html.
[39] MPC564EVB User's Manual, Freescale Semiconductor, Inc.
[40] MATLAB® R2007a Help.
[41] J. Ryu, M. Yoon, M. Sunwoo, Int. J. Automot. Technol. 7 (2006) 687–695.
[42] W. Lawrenz, CAN System Engineering From Theory to Practical Applications, Springer, 1997.